

Cause of the appearance of oxygen vacancies in yttria-stabilized zirconia and its relation to 2.8 eV photoluminescence

This content has been downloaded from IOPscience. Please scroll down to see the full text.

2015 Jpn. J. Appl. Phys. 54 06GC03

(<http://iopscience.iop.org/1347-4065/54/6S2/06GC03>)

View [the table of contents for this issue](#), or go to the [journal homepage](#) for more

Download details:

IP Address: 133.9.4.11

This content was downloaded on 16/11/2015 at 06:13

Please note that [terms and conditions apply](#).

Cause of the appearance of oxygen vacancies in yttria-stabilized zirconia and its relation to 2.8 eV photoluminescence

Shoji Kaneko^{1*}, Takaaki Morimoto¹, and Yoshimichi Ohki^{1,2*}

¹Department of Electrical Engineering and Bioscience, Waseda University, Shinjuku, Tokyo 169-8555, Japan

²Research Institute for Materials Science and Technology, Waseda University, Shinjuku, Tokyo 169-8555, Japan

E-mail: yohki@waseda.jp; s.kaneko.4869@akane.waseda.jp

Received November 27, 2014; accepted March 17, 2015; published online June 1, 2015

When we implanted P⁺ or B⁺ ions into yttria-stabilized zirconia (YSZ), its crystallinity was degraded. Concurrently, the photoluminescence at around 2.8 eV originating from two types of oxygen vacancies with one or two captured electrons became weak, indicating a decrease in the number of oxygen vacancies. Oxygen vacancies appear in YSZ as a result of the replacement of Zr⁴⁺ by Y³⁺ in ZrO₂. Therefore, it seems that the separation of YSZ into ZrO₂ and Y₂O₃ induced by the ion implantation is responsible for the decrease in the number of oxygen vacancies. Moreover, the intensity of the 2.8 eV photoluminescence returns to the value before the ion implantation if the sample is annealed thermally after the implantation at temperatures higher than the crystallization temperature of YSZ. The reaction opposite to the above seems to be induced by the thermal annealing. © 2015 The Japan Society of Applied Physics

1. Introduction

With the progress in the miniaturization of metal oxide semiconductor field-effect transistors in large-scale integrated circuits, the thickness of gate dielectrics become increasingly smaller, causing SiO₂ to become unsuitable for the gate dielectric, since it would become too thin to maintain its insulating property.^{1–3} One possible solution to this problem is to use other dielectric materials that possess higher dielectric constants (*k*).⁴

Although hafnium-based oxides have been extensively investigated,^{5–8} it is known that, in practical use, they form silicates if they are on a Si substrate.^{9,10} Regarding this problem, yttria-stabilized zirconia (YSZ), which possesses a high *k* of around 27,¹¹ is assumed to be promising for a future gate insulator.^{12,13} It has been reported that high-*k* dielectrics such as YSZ may have point defects.^{13–15} If this is the case, they would be a potential risk for their use in electronic devices.

Therefore, in this research, we examine what kinds of defects are present in YSZ, focusing particularly on oxygen vacancies. Photoluminescence (PL) was used as the main analytical tool in addition to the measurements of X-ray diffraction (XRD), electron spin resonance (ESR), and optical absorption, since these methods have been very effective for examining the structural changes induced in various inorganic insulating materials.^{6–8,16–36} We also use the implantation of ions as a method of damaging the crystalline structure and thermal annealing to recover the damaged structure.

2. Experimental methods

Commercially available YSZ (100) single-crystal samples, grown by the skull-melting method³⁷ (Crystal Base), were used in the experiments. They were cut to rectangular plates with a thickness of 0.5 mm. The proportions of yttria and zirconia are 9.8 and 90.2 mol %, respectively.

Positive monovalent ions of phosphorus (P⁺) or boron (B⁺) were implanted at room temperature, using the ion accelerator (Ulvac UP-150) at Waseda University, into the samples at an acceleration energy of 100 keV to various doses ranging from 0.2×10^{15} to 1.0×10^{15} cm⁻². After the ion implantation to the dose of 10^{15} cm⁻², the samples were

heated to various temperatures between 150 and 800 °C for 3 min in air and then kept at each annealing temperature for designated periods between 20 s and 20 min for annealing. Furthermore, for comparison, ultraviolet (UV) photons were irradiated to unimplanted samples for 30 min at room temperature using a KrCl excimer lamp (Ushio UER 20-222) that emits photons with an energy of 5.59 eV.

Before and after the ion implantation or thermal annealing, in-plane XRD spectra were obtained with Cu K α X-rays at room temperature using Rigaku Rint-Ultima III, while ESR spectra were obtained with JEOL JES-FA 300 at room temperature at 9.20 GHz (X band) using the microwave power of 5.00 mW. Optical absorption spectra in the visible-UV region were measured with a double-beam spectrophotometer (Shimadzu UV-3100PC) in the transmission mode at room temperature.

For PL measurements at 77 K, a fluorescence spectrometer (JASCO FP-8500) was used. Furthermore, PL spectra were also obtained at 10 K using synchrotron radiation (SR) to excite PLs at the BL3B line with a beam energy of 750 MeV equipped with a 2.5 m off-plane Eagle-type monochromator in the UVSOR Facility (Institute for Molecular Science, Okazaki, Japan). For the SR measurements, a 300 mm triple-grating monochromator (Acton SpectraPro-300i) was used as an incidence monochromator and a CCD camera (Princeton Instruments) was used to detect PLs. The intensity of PL was calibrated by taking into account the excitation SR intensity at each photon energy.

Moreover, the PL lifetime in the ms range was measured at 77 K using the FP-8500 spectrometer, whereas that in the ns range was measured at 10 K by a time-correlated single-photon counting technique using SR pulses. The SR pulse under a single-bunch mode has an apparent duration of about 550 ps including the time response of the detection system, and the time interval between two consecutive SR pulses is about 177.6 ns.³⁸

3. Results

First, we estimated how deep ions can penetrate into YSZ using a simulation program called SRIM2011.³⁹ As shown in Fig. 1, the projected ranges of P⁺ and B⁺ ions with an energy of 100 keV in YSZ are estimated to be about 80 and 200 nm, respectively. Compared with this, the depth

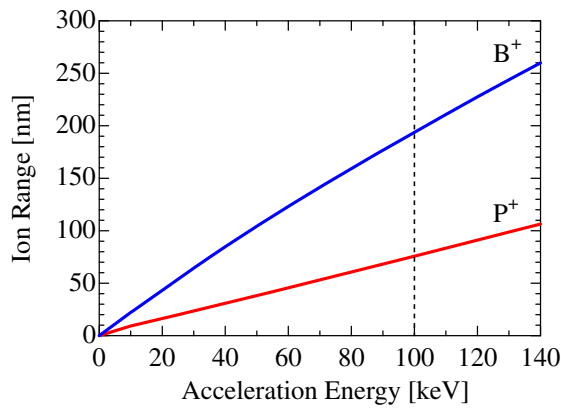


Fig. 1. (Color online) Projected ranges of P⁺ and B⁺ ions in YSZ.

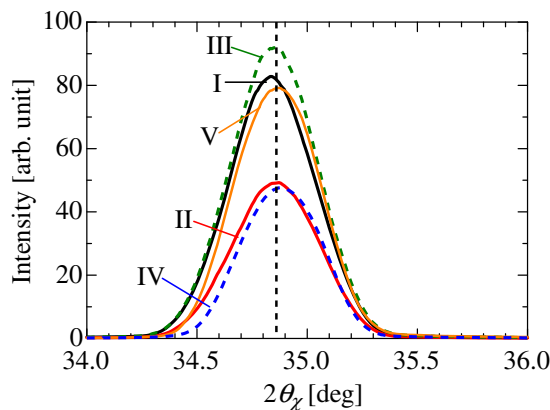


Fig. 2. (Color online) In-plane XRD patterns obtained for the following YSZ samples: I) untreated, II) implanted with P⁺ ions to a dose of 10¹⁵ cm⁻², III) annealed at 300 °C for 10 min following the implantation of P⁺ ions, IV) implanted with B⁺ ions to a dose of 10¹⁵ cm⁻², V) irradiated by photons with an energy of 5.59 eV for 30 min.

measurable using in-plane XRD is 2 to 8 nm.⁴⁰⁾ Here, we set the incident angle of X-rays to be 0.32° so that the diffraction intensity is maximum in YSZ. At this angle, the measurable depth is about 5 nm. Therefore, the depth measurable using XRD is much shallower than the projected ranges of ions with the energy of 100 keV.

Figure 2 shows the in-plane XRD spectra observed for samples treated by the following four procedures; implantation of P⁺ ions to a dose of 10¹⁵ cm⁻², implantation of B⁺ ions to the same dose, thermal annealing at 300 °C for 10 min after the P⁺ implantation, and UV irradiation with a photon energy of 5.59 eV for 30 min, along with the spectrum observed for the unimplanted sample. The unimplanted sample exhibits a peak at 2θ_χ = 34.9°, which corresponds to the diffraction by crystalline YSZ at its (200) planes. The intensity of the XRD peak is decreased by the implantation of P⁺ or B⁺ ions, as shown by curve II or IV. The thermal annealing at 300 °C that followed the P⁺ ion implantation returns the intensity to nearly the same strength as that of the unimplanted sample. On the other hand, the UV irradiation given to the untreated sample does not change the XRD intensity.

Figure 3 shows ESR spectra observed for the above five samples. As indicated by curves II and IV in Fig. 3(a), two ESR signals appear at g = 2.00 and 1.97 after the implantation of P⁺ or B⁺ ions to the dose of 10¹⁵ cm⁻²,

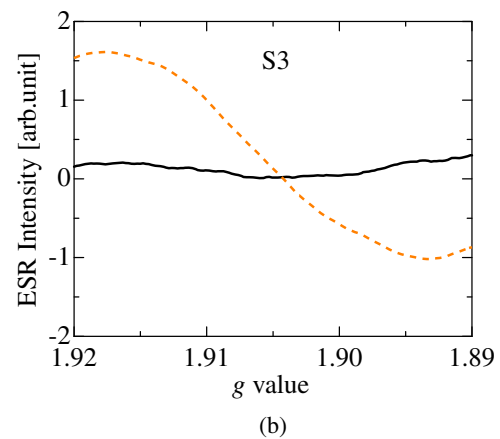
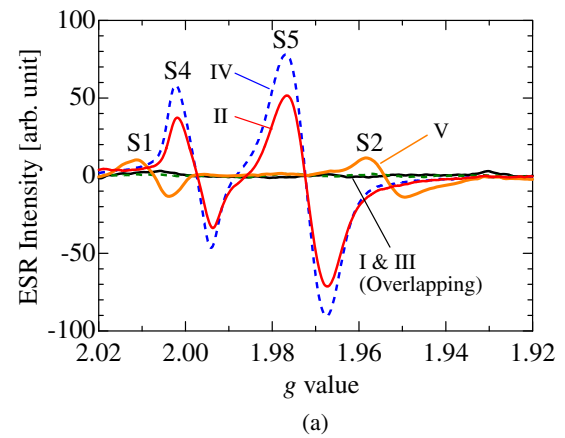


Fig. 3. (Color online) (a) ESR spectra obtained for the following YSZ samples: I) untreated, II) implanted with P⁺ ions to a dose of 10¹⁵ cm⁻², III) annealed at 300 °C for 10 min following the implantation of P⁺ ions, IV) implanted with B⁺ ions to a dose of 10¹⁵ cm⁻², V) irradiated by photons with an energy of 5.59 eV for 30 min. (b) ESR spectra observed before (black solid) and after the irradiation of 5.59 eV photons (orange dashed).

whereas they disappear after the following thermal annealing at 300 °C for 10 min. In the present paper, the above two ESR signals at g = 2.00 and 1.97 are referred to as S4 and S5, respectively. On the other hand, as shown in Figs. 3(a) and 3(b), three ESR signals appear after UV irradiation with a photon energy of 5.59 eV for 30 min at g = 2.006, 1.97–1.95, and 1.91–1.86, which were referred to as S1, S2, and S3, respectively, in our previous paper.³⁰⁾

Figure 4(a) shows optical absorption spectra observed for the samples untreated and treated in the same manner as those in the cases of Figs. 2 and 3, while Fig. 4(b) shows their differential spectra after each treatment. After the implantation of P⁺ or B⁺ ions to the dose of 10¹⁵ cm⁻², an absorption band appears at around 2.4 eV, which disappears after the following thermal annealing at 300 °C. On the other hand, UV irradiation of the untreated sample with a photon energy of 5.59 eV for 30 min yields a small and broad absorption band at around 3.3 eV.³⁰⁾

Figure 5(a) shows PL spectra observed for the samples untreated and treated in the same manner as above. They were excited by 5.2 eV photons and measured at 77 K using the fluorescence spectrometer FP-8500. As indicated by spectrum I, the unimplanted sample exhibits a peak at around 2.8 eV. The intensity of the 2.8 eV PL peak is decreased by the implantation of P⁺ or B⁺ ions, as shown in spectrum II or

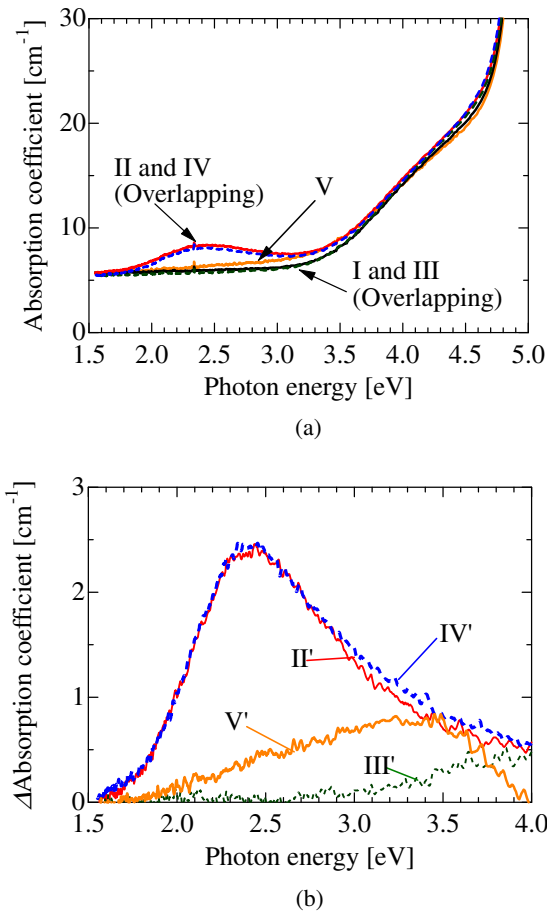


Fig. 4. (Color online) (a) Optical absorption spectra obtained for the following YSZ samples: I) untreated, II) implanted with P⁺ ions to a dose of 10¹⁵ cm⁻², III) annealed at 300 °C for 10 min following the implantation of P⁺ ions, IV) implanted with B⁺ ions to a dose of 10¹⁵ cm⁻², V) irradiated by photons with an energy of 5.59 eV for 30 min. (b) Curves II', III', IV', and V' represent the increments in absorption coefficient obtained by subtracting curve I from curves II, III, IV, and V, respectively.

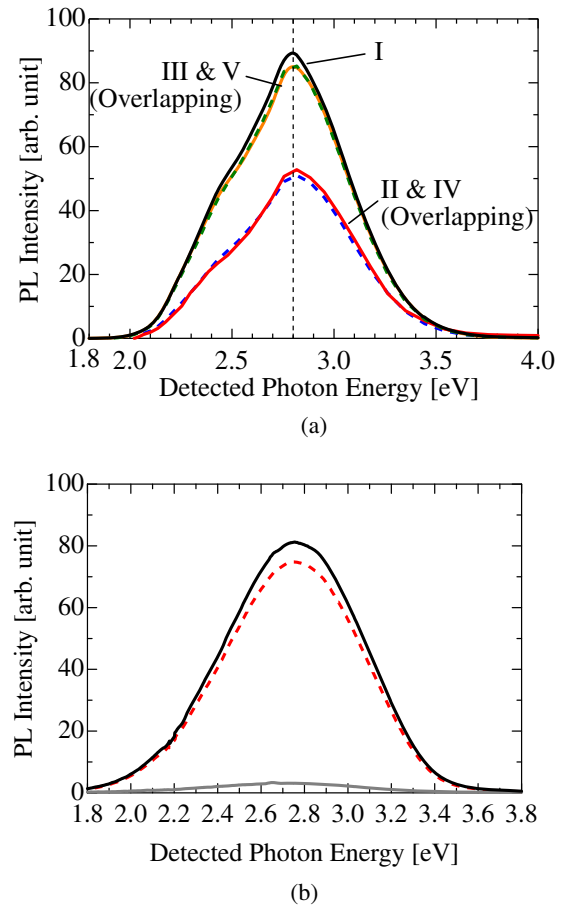


Fig. 5. (Color online) (a) 2.8 eV PL spectra at 77 K excited by 5.2 eV photons obtained for the following YSZ samples: I) untreated, II) implanted with P⁺ ions to a dose of 10¹⁵ cm⁻², III) annealed at 300 °C for 10 min following the implantation of P⁺ ions, IV) implanted with B⁺ ions to a dose of 10¹⁵ cm⁻², V) irradiated by photons with an energy of 5.59 eV for 30 min. (b) PL spectra observed in untreated YSZ at 10 (black solid), 77 (red dashed), and 300 K (gray solid).

IV, whereas it returns to a similar strength to its original value upon the following annealing at 300 °C. On the other hand, UV irradiation does not yield any change, as shown by spectrum V. This dependence of the 2.8 eV PL on the treatment given to the sample is similar to that of the XRD intensity shown in Fig. 2. Figure 5(b) shows the temperature dependence of the intensity of the 2.8 eV PL excited by 5.2 eV photons, measured at 10, 77, and 300 K using SR. The PL intensity decreases with increasing temperature.

Figure 6 shows the effects of the dose of implanted P⁺ ions on the intensities of the above-mentioned various physical features. With the increase in dose, two ESR signals, S4 and S5, and optical absorption at 2.4 eV increase monotonically, while the XRD and the broad PL at 2.8 eV show a monotonic decrease.

We conducted a similar study on the effects of ion implantation using two high-*k* dielectrics, LaAlO₃ and YAlO₃.^{35,36} Therefore, PL spectra of YSZ observed at 10 K before and after the implantation of P⁺ ions to the dose of 10¹⁵ cm⁻² are shown in Fig. 7 with those of LaAlO₃ and YAlO₃. Here, the PLs were excited by photons with energies of 5.2 eV for YSZ, 5.0 eV for LaAlO₃, and 5.6 eV for YAlO₃, so that the intensity of the 2.8 eV PL became maximum. A very broad PL is seen in all the samples at around 2.8 eV.

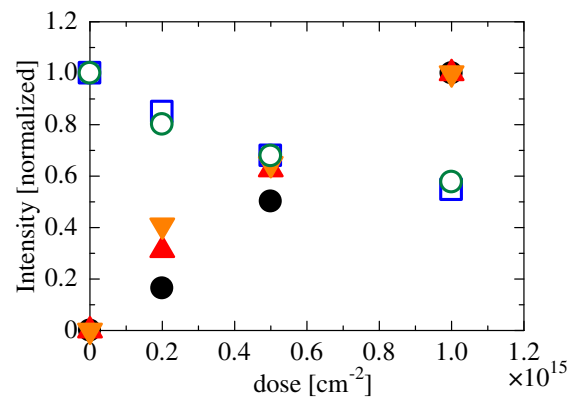


Fig. 6. (Color online) Effects of the implanted dose of P⁺ ions on the intensities of the two ESR signals S4 at *g* = 2.00 (red closed triangles) and S5 at *g* = 1.97 (orange inverted closed triangles) and the absorption band at 2.4 eV (black closed circles), normalized by respective intensities observed right after the implantation to a dose of 10¹⁵ cm⁻² into YSZ, together with the dose-dependent decrease in XRD peak intensity (blue open squares) and that of the 2.8 eV PL intensity excited by 5.2 eV photons (green open circles), normalized by their intensities before the implantation.

One important thing here is that the ordinate differs among (a), (b), and (c) and that the PL intensity is very strong in YSZ compared with those in LaAlO₃ and YAlO₃. Another

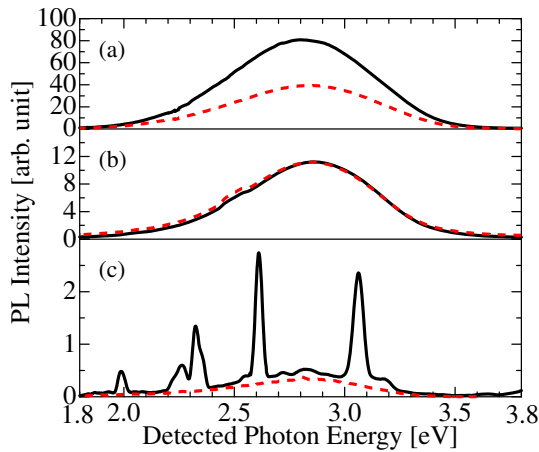


Fig. 7. (Color online) PL spectra at 10K observed in (a) YSZ, (b) LaAlO₃, and (c) YAlO₃ before (black solid) and after the P⁺ ion implantation (red dashed).

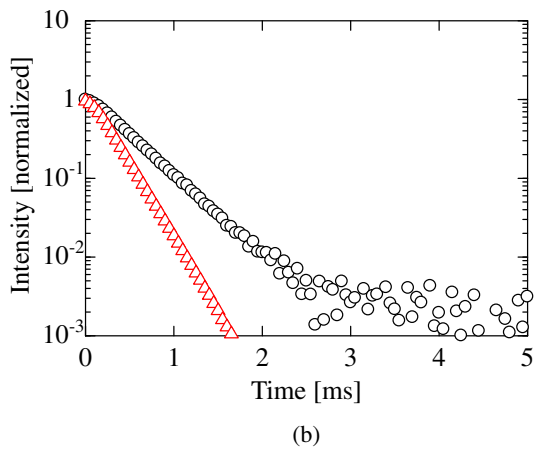
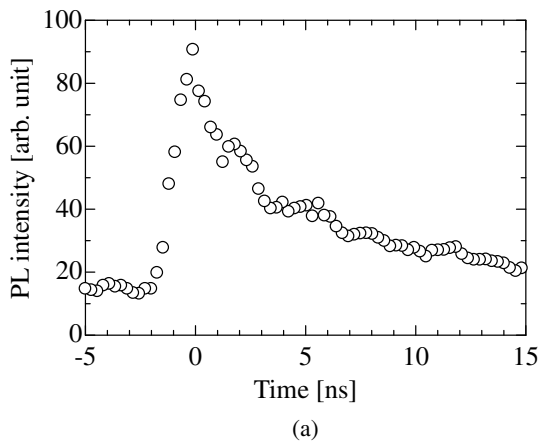


Fig. 8. (Color online) (a) 2.8-eV PL decay profile in the ns range observed in untreated YSZ. (b) 2.8-eV PL decay profile in the ms range observed in untreated YSZ (black open circles), and the decay of excitation photons with an energy of 5.2 eV (red open triangles), normalized by their respective initial values.

important thing is that the PL intensity decreases substantially in YSZ upon ion implantation, although it negligibly changes in LaAlO₃ and YAlO₃. Note that several sharp peaks appearing in YAlO₃ will be discussed later.

Figure 8(a) shows the decay of the 2.8 eV PL observed in the unimplanted YSZ when it was excited by repeated pulses

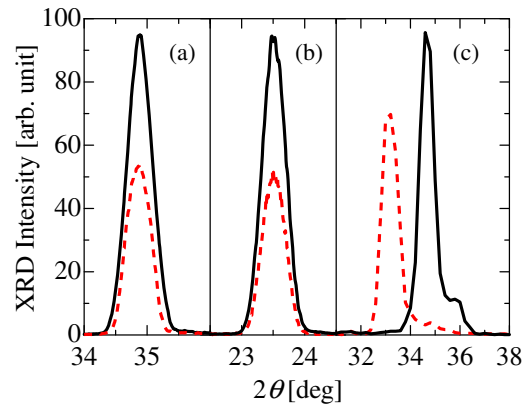


Fig. 9. (Color online) In-plane XRD patterns observed in (a) YSZ, (b) LaAlO₃, and (c) YAlO₃ before (black solid) and after the P⁺ ion implantation (red dashed).

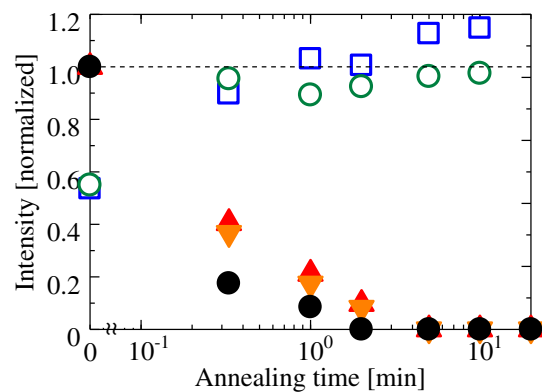


Fig. 10. (Color online) Time-dependent decay profiles of the intensities of the ion-induced ESR signals S4 at $g = 2.00$ (red closed triangles) and S5 at $g = 1.97$ (orange inverted closed triangles) and the absorption band at 2.4 eV (black closed circles) during annealing at 300 °C, normalized by their intensities right after the implantation of P⁺ ions to a dose of 10¹⁵ cm⁻², together with the recovery of the XRD peak intensity (blue open squares) and that of the 2.8 eV PL intensity (green open circles), normalized by their intensities before the implantation.

of 5.2 eV SR photons in the single-bunch mode. From this decay, the decay constant of the 2.8 eV PL can be calculated to be 7 ns. Figure 8(b) shows the decay of the 2.8 eV PL in the unimplanted YSZ when it was excited at 5.2 eV using the fluorescence spectrometer FP-8500. The weakening of the intensity of the excitation photons as a function of time owing to the movement of a mechanical shutter is also shown. From this decay, it can be estimated that the 2.8 eV PL also has a slow component with a decay constant of around 0.3 ms.

Figure 9 shows in-plane XRD spectra observed before and after the implantation of P⁺ ions to a dose of 10¹⁵ cm⁻² for YSZ (a), LaAlO₃ (b), and YAlO₃ (c).^{35,36} The intensities of the XRD spectral peaks are decreased upon ion implantation in the three high- k dielectrics.

Figure 10 shows the effects of the thermal annealing period at 300 °C for designated periods ranging from 20 s to 20 min after the implantation of P⁺ ions to the dose of 10¹⁵ cm⁻². The two ESR signals, S4 and S5, and the absorption at 2.4 eV, which were induced by the ion implantation, decrease promptly and they disappear in 5 min. Furthermore, the intensities of the XRD peak and the 2.8 eV PL, which became

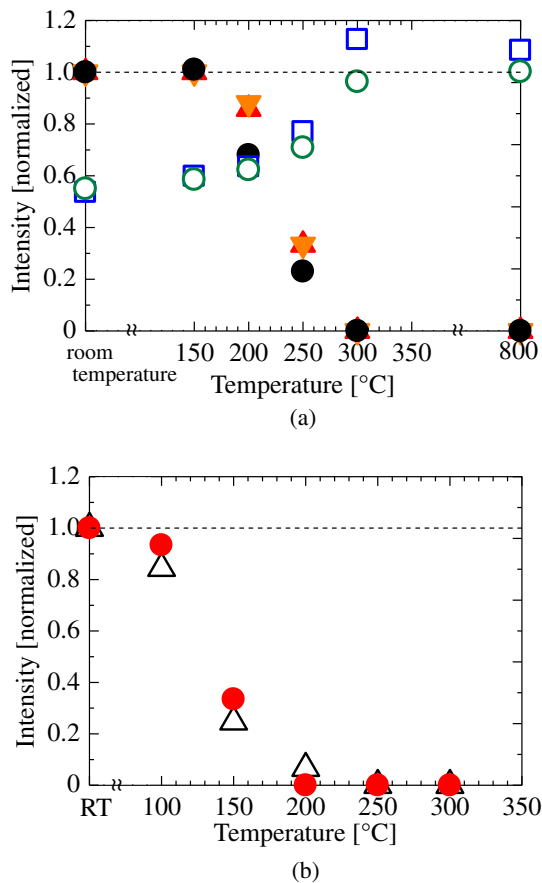


Fig. 11. (Color online) (a) Decay profiles of the intensities of the ion-induced ESR signals S4 at $g = 2.00$ (red closed triangles) and S5 at $g = 1.97$ (orange inverted closed triangles) and the absorption band at 2.4 eV (black closed circles) after annealing at various temperatures for 10 min, normalized by their intensities right after the implantation of P^+ ions to a dose of 10^{15} cm^{-2} , together with the recovery of the XRD peak intensity (blue open squares) and that of the 2.8 eV PL intensity (green open circles), normalized by their intensities before the implantation. (b) Similar changes in the photon-induced ESR signal S2 at $g = 1.97\text{--}1.95$ (black open triangles) and absorption band at 3.3 eV (red closed circles), normalized by their intensities right after the irradiation of photons with an energy of 5.59 eV for 30 min.

smaller after ion implantation, recover completely in 5 min to the values before ion implantation.

Figure 11(a) shows the effects of the temperature of annealing for 10 min between 150 and 800 °C after the implantation of P^+ ions to a dose of 10^{15} cm^{-2} . With the increase in annealing temperature, the two ESR signals and the optical absorption at 2.4 eV, which were induced by the ion implantation, show a monotonic decrease and they disappear at 300 °C. In contrast, the XRD peak and the 2.8 eV PL, which became weaker after the implantation, increase back to their original values. Although the data are not shown here, the two ESR signals, S4 and S5, the absorption at 2.4 eV, the XRD peak, and the 2.8 eV PL exhibit essentially the same recovery behavior after annealing at 300 °C for 10 min following the implantation of B^+ ions to the same dose.

A similar annealing was conducted for 10 min on the unimplanted samples after they had been irradiated by UV photons with an energy of 5.59 eV for 30 min. Figure 11(b) shows the effects of the annealing temperature on the ESR signal S2 and the absorption at 3.3 eV. Both the ESR signal and the absorption, which were induced by the UV

irradiation, decrease to less than 40% at 150 °C and disappear at 200 °C. Therefore, Fig. 11 clearly shows that reactions exactly opposite to those induced by ion implantation or by UV irradiation are induced by thermal annealing for all the above-mentioned phenomena. Note that annealing experiments could not be performed for the two photoinduced ESR signals S1 and S3, because S1 decreases immediately, even at room temperature, and S3 is too weak.

4. Discussion

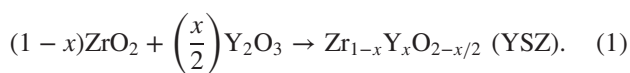
In YSZ, an oxygen vacancy that captures one electron (F^+ center) and an oxygen vacancy that captures no electrons (F^{2+} center) are known to form a defect pair, namely, the F^+F^{2+} pair.⁴¹⁾ Judging from their anisotropic nature and g values,⁴¹⁾ the two ESR signals S4 and S5 shown in Fig. 3(a), which are induced by ion implantation, seem to be due to the F^+F^{2+} pair. Note that ESR cannot detect the single presence of F^{2+} centers or F centers (oxygen vacancies with two captured electrons). As for the absorption at 2.4 eV induced by the ion implantation (Fig. 4), a very similar absorption has been attributed to F^+ centers,⁴¹⁾ although it was still uncertain in Ref. 41 whether the F^+ centers were present alone or in the form of the above-mentioned F^+F^{2+} pair. As shown in Fig. 6, the two ESR signals, S4 and S5, and the absorption at 2.4 eV show a monotonic increase with increasing dose of the implanted P^+ ions. This means that the ion implantation induces ionization or the generation of electron–hole pairs to change the charging state of oxygen vacancies. On the other hand, the monotonic decrease in the intensity of the XRD peak with increasing dose of the implanted ions shown in Fig. 6 indicates the collapse of the crystalline structure. By taking this into account, it can be summarized that the ion implantation induces the generation of electron–hole pairs and the deformation of the crystalline structure.

As for the 2.8 eV PL, PL similar to the one shown in Fig. 5 has been ascribed to oxygen vacancies without mentioning their details⁴²⁾ or to the F^+ centers.⁴³⁾ The intensity of this PL decreases significantly with the increase in temperature, as shown in Fig. 5(b). Furthermore, the 2.8 eV PL has a decay constant of about 7 ns, as shown in Fig. 8(a), indicating that it is fluorescence. In addition to this fast component, the PL has a slow component with a decay constant of about 0.3 ms, as shown in Fig. 8(b).

In alumina,⁴⁴⁾ MgO ,⁴⁵⁾ and $YAlO_3$,⁴⁶⁾ it has been reported that the F centers produce phosphorescence with a time constant of the order of ms, while the F^+ centers have been assigned to the luminophore of the fluorescence with a time constant of the order of ns. Taking these facts into account, the 2.8 eV PL in YSZ would be ascribable to both the F^+ and F centers. However, it is not plausible that both the F^+ and F centers with different charging states emit photons with the same energy. Regarding this, we assume the following luminescent mechanism to be a plausible model. Namely, the 2.8 eV PL in YSZ is induced by the F^+ centers with the decay constant of 7 ns. One important fact is that the F^+ centers can be generated if one electron is released from the F centers in addition to those originally present in YSZ. If this electron release requires some time, the 2.8 eV PL must have a large decay constant such as 0.3 ms if it originates from the F centers. Note that a similar PL due to F centers in alumina has a large decay constant of about 30 ms.⁴⁴⁾

The PL that is ascribed to oxygen vacancies has been observed in many oxides such as YSZ,^{42,43} silica glass,^{19,21,25} Ge-doped silica glass,²⁴ buried SiO₂ in Si,^{22,23} and alumina,^{44,46,47} as well as in silicon nitride²⁶ and several aluminates such as LaAlO₃^{31,32,35,36} and YAlO₃.^{35,36,46,47} Except for YSZ, namely, the target material of the present research, the PL due to the oxygen vacancies appears regardless of the sample being crystalline or amorphous. For example, the PL is clearly observed in completely amorphous SiO₂ deposited by a soot remelting method²¹ or by thermal oxidation.^{22,48} Moreover, although many types of PL appearing in LaAlO₃ and YAlO₃ become weak if the crystallinity of the sample becomes poor, only the intensity of the PL due to the oxygen vacancies does not decrease,^{35,36} which is also shown in Fig. 7. Therefore, the strong dependence of the 2.8 eV PL in YSZ on the crystallinity of the sample, which can be seen in Figs. 5, 6, 7(a), 10, and 11(a), is exceptional. Namely, its intensity becomes weak upon the implantation of P⁺ ions in a similar manner to the decrease in crystallinity. Compared with YSZ, the intensity of the corresponding PL does not decrease in LaAlO₃ or YAlO₃ after the implantation, although the crystallinity of the two aluminates degrades similarly to that of YSZ. Furthermore, the PL intensity of YSZ is more than ten times as intense as the corresponding PL in LaAlO₃ and YAlO₃, as shown in Fig. 7. In addition, the ESR signals S1, S4, and S5, which indicate the existence of the F⁺ centers, appear in YSZ after the ion implantation, as shown in Fig. 3. In more detail, signal S1 is due to F⁺ centers³⁰ and the two signals S4 and S5 are both due to the F⁺-F²⁺ pair.⁴¹ In contrast to this, F⁺ centers were not observed in LaAlO₃ or YAlO₃ when we performed similar experiments under the same conditions using the same spectrometer.

Oxygen vacancies appear in oxides such as silica or in aluminates such as LaAlO₃ and YAlO₃ only when their crystals have defects. However, YSZ is a kind of ZrO₂ in which Zr⁴⁺ is replaced by Y³⁺, as shown by the following chemical formula:⁴⁹



This means that YSZ has the same number of oxygen vacancies as that of the incorporated Y₂O₃.⁴¹ Therefore, many more oxygen vacancies exist in YSZ than in LaAlO₃ and YAlO₃.

It has been shown that the temperature of a path in a dielectric substance along which an ion passes increases to about 3000 °C, taking SiO₂ as an example.⁵⁰ If ZrO₂ and Y₂O₃ are locally formed in YSZ through the opposite reaction of Eq. (1) upon the implantation of ions as a result of such a high temperature, the crystallinity should become poor and the number of oxygen vacancies should decrease. This is the reason for the decrease in the intensity of the 2.8 eV PL upon the degradation of crystallinity.

On the other hand, as shown in Fig. 4, the absorption band appears after the implantation of P⁺ or B⁺ ions at around 2.4 eV, which is near the energy of the 2.8 eV PL. There is a possibility that the 2.8 eV PL is absorbed by this absorption band and thus its intensity is measured as being lower than its true intensity. Regarding this, the absorption of photons at 2.8 eV can be calculated to be 2.3% on the assumption that the

2.8 eV PL was emitted at a depth of 100 μm from the sample surface. This means that the effect of the increase in absorption at 2.4 eV after the ion implantation on the intensity of the 2.8 eV PL is negligible. Therefore, the decrease in the intensity of the 2.8 eV PL induced after the ion implantation is ascribable to the decrease in the number of the oxygen vacancies induced by the opposite reaction of Eq. (1). Namely, the PL intensity decreases as a result of the partial separation of YSZ to ZrO₂ and Y₂O₃. Although this separation of YSZ induces the degradation of the crystallinity of YSZ, it is not the direct reason for the decrease in the PL intensity.

As shown by curve V in Fig. 3, three ESR signals, S1, S2, and S3, are induced in YSZ upon the irradiation of UV photons with an energy of 5.59 eV. Here, S1 is due to the F⁺ center, while S3 is due to the T center or two oxygen vacancies on two diagonal sites adjacent to Zr³⁺.³⁰ The origin of S2 is unknown. The F⁺ centers induced by the UV irradiation exist alone without forming a defect pair like the above-mentioned F⁺-F²⁺ center, since it does not show anisotropy. On the other hand, a broad absorption increase with a peak at around 3.3 eV, indicated by curve V or V' in Fig. 4, induced by the irradiation of UV photons, is considered to be due to the T center.^{30,41} This assignment indicates that the charging state of oxygen vacancies is changed upon the irradiation of the UV photons.

Neither the XRD peak shown in Fig. 2 nor the 2.8 eV PL due to both the F⁺ and F centers shown in Fig. 5(a) exhibits a meaningful change upon the irradiation of UV photons. As mentioned above, the 2.8 eV PL appears bright if the sample contains oxygen vacancies in the form of O_{2-x/2} in the right-hand term of Eq. (1). From these results, shown in Figs. 2–5, the irradiation of UV photons seems to induce the generation of electron–hole pairs, but not the opposite reaction of Eq. (1) or the deformation of the crystallinity of YSZ. This is in strong contrast to the changes induced in YSZ upon the implantation of ions.

As shown in Figs. 2–5, 10, and 11, reactions opposite to those caused by the implantation of ions are induced by the thermal annealing performed successively after the implantation. Namely, the intensities of the XRD peak and the 2.8 eV PL, which were decreased by the ion implantation, increase back to their original values after the thermal annealing. Furthermore, two ESR signals, S4 and S5, and the absorption at 2.4 eV, which were induced by the ion implantation, become weak. In addition, the five physical quantities shown in Fig. 10 mutually correlate very well with respect to the dependence on the annealing time at 300 °C. Moreover, these quantities return to the values before the ion implantation when the sample is annealed at 300 °C for 5 min. Note that they also mutually correlate very well regarding the dose dependence of the implantation of P⁺ ions shown in Fig. 6. As shown in Fig. 11(a), the annealing at temperatures higher than 300 °C, which is the crystallization temperature of YSZ,⁵¹ is needed to return the five physical quantities back to their values before the ion implantation when the annealing period is 10 min.

Although the data are not shown, the ESR signal S1 at $g = 2.006$ shown in Fig. 3(a), which is due to the single F⁺ centers induced by the irradiation of photons with an energy of 5.59 eV for 30 min, decreases rapidly even at room temperature.³⁰ Furthermore, as mentioned above, the appear-

ance of the ESR signal S2 and the absorption at 3.3 eV owing to the T centers indicate that the charging states of defects in YSZ are changed by the irradiation of photons at 5.59 eV for 30 min. As shown in Fig. 11(b), the two quantities begin to decrease at 100 °C and disappear at 200 °C in 10 min. Namely, the signals S1 and S2 and the absorption at 3.3 eV, induced by the UV irradiation, disappear more easily than the signals S4 and S5 and the absorption at 2.4 eV induced by the implantation of ions. The reason for this is simply that the change in the charging state of oxygen vacancies induced by UV irradiation is caused by photoionization or photo-generated electrons and holes, whereas the implantation of ions causes the degradation of crystallinity or the reaction opposite to Eq. (1) and the resultant disappearance of oxygen vacancies. Therefore, the changes induced by the UV irradiation are relaxed at low annealing temperatures, whereas those induced by ions need high temperatures. It has also been reported for crystalline silica that the recovery of crystalline damage needs temperatures as high as 1000 °C, while the change in the charging states can be recovered at 200 °C.^{52,53)}

Note that sharp PL peaks appearing at 2.3, 2.6, and 3.1 eV in YAlO₃ [Fig. 7(c)] are ascribable to Er³⁺,^{35,36)} judging from their energies.⁵⁴⁾ Since Er is a rare-earth element similarly to Y, it would be easily included in YAlO₃ as an impurity. Moreover, the shift in the angle of the XRD peak appearing only in YAlO₃, shown in Fig. 9(c), is attributable to elemental displacement caused by the implantation of ions.^{35,36)} The reason for this shift being observed only in YAlO₃ is unclear, but it may indicate that YAlO₃ is more easily subject to ion implantation.

In addition, as mentioned above, the presence of oxygen vacancies in LaAlO₃ and YAlO₃ can be detected by PL, as shown in Fig. 7, while it is not detectable by ESR. This indicates that the sensitivity of PL measurements is fairly high. Although only the F⁺ center with one captured electron is detectable by ESR, which can detect only radicals, both the F⁺ and F centers contribute to the 2.8 eV PL. This seems to make the PL measurements more suitable to the detection of oxygen vacancies than ESR.

5. Conclusions

The effects of ion implantation and thermal annealing on the formation of point defects in YSZ were analyzed experimentally by obtaining spectra of in-plane XRD, ESR, optical absorption in the visible-UV region, and PL. Important results obtained are summarized as follows.

- 1) The presence of oxygen vacancies was confirmed as point defects in YSZ.
- 2) After the ion implantation, the charging state of oxygen vacancies is changed. This generates two ESR signals at $g = 2.00$ and 1.97 and optical absorption at 2.4 eV, which are ascribable to the F⁺-F²⁺ pair and the F⁺ center, respectively. Concurrently, the crystalline structure of YSZ collapses and the intensity of the 2.8 eV PL due to both the F⁺ and F centers decreases.
- 3) The intensity of the 2.8 eV PL is very strong, since the oxygen vacancies are present in YSZ as a result of the replacement of Zr⁴⁺ by Y³⁺. The intensity is decreased significantly after the ion implantation, concurrently with the degradation of crystallinity. This suggests that

the number of oxygen vacancies is decreased as a result of the separation of ZrO₂ and Y₂O₃ upon the ion implantation.

- 4) When YSZ is exposed to UV photons at 5.59 eV, two ESR signals at $g = 2.006$ ascribable to the F⁺ center and at 1.91–1.86 ascribable to the T center increase. An unknown signal at 1.97–1.95 also increases. The strength of the optical absorption at 3.3 eV due to the T center also shows an increase. However, neither the crystallinity nor the 2.8 eV PL exhibits a meaningful change. These results indicate that only the charging state of oxygen vacancies is changed.
- 5) Because of the above-mentioned difference between the effects of ion implantation and UV irradiation, a higher temperature is required to recover the damage induced by ion implantation than the temperature needed to repair the changes induced by UV irradiation.

Acknowledgments

This study was partly conducted in the UVSOR Facility, Institute for Molecular Science, Okazaki, Japan. It was partly supported by a Mitsubishi Materials Corporation Grant from Waseda Research Institute for Science and Engineering.

- 1) D. A. Muller, T. Sorsch, S. Moccio, F. H. Baumann, K. Evans-Lutterodt, and G. Timp, *Nature* **399**, 758 (1999).
- 2) D. A. Neumayer and E. Cartier, *J. Appl. Phys.* **90**, 1801 (2001).
- 3) B. Brar, G. D. Wilk, and A. C. Seabaugh, *Appl. Phys. Lett.* **69**, 2728 (1996).
- 4) G. D. Wilk, R. M. Wallace, and J. M. Anthony, *J. Appl. Phys.* **87**, 484 (2000).
- 5) M. Matsuoka, S. Isotani, J. F. D. Chubaci, S. Miyake, Y. Setsuhara, K. Ogata, and N. Kuratani, *J. Appl. Phys.* **88**, 3773 (2000).
- 6) H. Kato, T. Nango, T. Miyagawa, T. Katagiri, K. S. Seol, and Y. Ohki, *J. Appl. Phys.* **92**, 1106 (2002).
- 7) T. Ito, M. Maeda, K. Nakamura, H. Kato, and Y. Ohki, *J. Appl. Phys.* **97**, 054104 (2005).
- 8) T. Ito, H. Kato, and Y. Ohki, *J. Appl. Phys.* **99**, 094106 (2006).
- 9) B. K. Park, J. Park, M. Cho, C. S. Hwang, K. Oh, Y. Han, and D. Y. Yang, *Appl. Phys. Lett.* **80**, 2368 (2002).
- 10) M. Quevedo-Lopez, M. El-Bouanani, S. Addepalli, J. L. Duggan, B. E. Gnade, R. M. Wallace, M. R. Visokay, M. Douglas, and L. Colombo, *Appl. Phys. Lett.* **79**, 4192 (2001).
- 11) D. K. Fork, D. B. Fenner, G. A. N. Connell, J. M. Phillips, and T. H. Geballe, *Appl. Phys. Lett.* **57**, 1137 (1990).
- 12) K. J. Hubbard and D. G. Schlom, *J. Mater. Res.* **11**, 2757 (1996).
- 13) J. Zhu and Z. G. Liu, *Mater. Lett.* **57**, 4297 (2003).
- 14) V. M. Orera, R. I. Merino, Y. Chen, R. Cases, and P. J. Alonso, *Phys. Rev. B* **42**, 9782 (1990).
- 15) J. P. Goff, W. Hayes, S. Hull, M. T. Hutchings, and K. N. Clausen, *Phys. Rev. B* **59**, 14202 (1999).
- 16) H. Nishikawa, R. Tohmon, Y. Ohki, K. Nagasawa, and Y. Hama, *J. Appl. Phys.* **65**, 4672 (1989).
- 17) S. Munekuni, T. Yamanaka, Y. Shimogaichi, R. Tohmon, Y. Ohki, K. Nagasawa, and Y. Hama, *J. Appl. Phys.* **68**, 1212 (1990).
- 18) S. Munekuni, N. Dohguchi, H. Nishikawa, Y. Ohki, K. Nagasawa, and Y. Hama, *J. Appl. Phys.* **70**, 5054 (1991).
- 19) H. Nishikawa, T. Shiroyama, R. Nakamura, Y. Ohki, K. Nagasawa, and Y. Hama, *Phys. Rev. B* **45**, 586 (1992).
- 20) H. Nishikawa, R. Nakamura, Y. Ohki, and Y. Hama, *Phys. Rev. B* **48**, 15584 (1993).
- 21) H. Nishikawa, E. Watanabe, D. Ito, and Y. Ohki, *Phys. Rev. Lett.* **72**, 2101 (1994).
- 22) K. S. Seol, Y. Ohki, H. Nishikawa, M. Takiyama, and Y. Hama, *J. Appl. Phys.* **80**, 6444 (1996).
- 23) K. S. Seol, A. Ieki, Y. Ohki, H. Nishikawa, and M. Tachimori, *J. Appl. Phys.* **79**, 412 (1996).
- 24) M. Fujimaki, Y. Ohki, and H. Nishikawa, *J. Appl. Phys.* **81**, 1042 (1997).
- 25) K. S. Seol, M. Fujimaki, Y. Ohki, and H. Nishikawa, *Phys. Rev. B* **59**, 1590

- (1999).
- 26) K. S. Seol, T. Futami, T. Watanabe, Y. Ohki, and M. Takiyama, *J. Appl. Phys.* **85**, 6746 (1999).
- 27) K. S. Seol, T. Watanabe, M. Fujimaki, H. Kato, Y. Ohki, and M. Takiyama, *Phys. Rev. B* **62**, 1532 (2000).
- 28) H. Kato, A. Masuzawa, H. Sato, T. Noma, K. S. Seol, M. Fujimaki, and Y. Ohki, *J. Appl. Phys.* **90**, 2216 (2001).
- 29) H. Kato, N. Kashio, Y. Ohki, K. S. Seol, and T. Noma, *J. Appl. Phys.* **93**, 239 (2003).
- 30) T. Morimoto, M. Takase, T. Ito, H. Kato, and Y. Ohki, *Jpn. J. Appl. Phys.* **47**, 6858 (2008).
- 31) K. Kanai, E. Hirata, and Y. Ohki, *Jpn. J. Appl. Phys.* **47**, 7980 (2008).
- 32) E. Hirata, K. Tamagawa, and Y. Ohki, *Jpn. J. Appl. Phys.* **49**, 091102 (2010).
- 33) D. Yamasaka, K. Tamagawa, and Y. Ohki, *J. Appl. Phys.* **110**, 074103 (2011).
- 34) D. Yamasaka, Y. Horii, T. Morimoto, and Y. Ohki, *Jpn. J. Appl. Phys.* **52**, 071501 (2013).
- 35) T. Morimoto, Y. Horii, M. Harima, and Y. Ohki, presented at 61st JSAP Spring Meet., 2014, 20a-F11-9 [in Japanese].
- 36) T. Morimoto, Y. Horii, T. Inoue, S. Kaneko, M. Harima, and Y. Ohki, *Hoden Kenkyu* **57**, 3 (2014) [in Japanese].
- 37) G. Dhanaraj, K. Byrappa, V. Prasad, and M. Dudley, *Springer Handbook of Crystal Growth* (Springer, Berlin, 2010) p. 433.
- 38) K. Kan'no, K. Tanaka, T. Mukai, Y. Nakai, M. Itoh, T. Miyayama, K. Fukui, and M. Watanabe, *Phys. Scr.* **41**, 120 (1990).
- 39) Web [<http://www.srim.org/SRIM/SRIM2011.htm>].
- 40) Web [http://henke.lbl.gov/optical_constants/atten2.html].
- 41) J. M. Costantini, F. Beuneu, and W. J. Weber, *J. Nucl. Mater.* **440**, 508 (2013).
- 42) H. Nakajima and T. Mori, *J. Alloys Compd.* **408–412**, 728 (2006).
- 43) N. G. Petrik, D. P. Taylor, and T. M. Orlando, *J. Appl. Phys.* **85**, 6770 (1999).
- 44) A. I. Surdo, V. S. Kortov, and V. A. Pustovarov, *Radiat. Meas.* **33**, 587 (2001).
- 45) G. H. Rosenblatt, M. W. Rowe, G. P. Williams, Jr., R. T. Williams, and Y. Chen, *Phys. Rev. B* **39**, 10309 (1989).
- 46) Y. V. Zorenko, A. S. Voloshinovskii, and I. V. Konstankevych, *Opt. Spectrosc.* **96**, 532 (2004).
- 47) A. I. Popov, E. A. Kotomin, and J. Maier, *Nucl. Instrum. Methods Phys. Res., Sect. B* **268**, 3084 (2010).
- 48) K. H. Lee, C. Lofton, K. Kim, W. S. Seo, Y. Lee, M. H. Lee, and W. Sigmund, *Solid State Commun.* **131**, 687 (2004).
- 49) K. C. Lau and B. I. Dunlap, *J. Phys.: Condens. Matter* **23**, 035401 (2011).
- 50) K. Awazu, X. Wang, M. Fujimaki, J. Tominaga, H. Aiba, Y. Ohki, and T. Komatsubara, *Phys. Rev. B* **78**, 054102 (2008).
- 51) J. Yang, J. Lian, Q. Dong, Q. Guan, J. Chen, and Z. Guo, *Mater. Lett.* **57**, 2792 (2003).
- 52) P. J. Chandler, L. Zhang, and P. D. Townsend, *Nucl. Instrum. Methods Phys. Res., Sect. B* **46**, 69 (1990).
- 53) P. D. Townsend, P. J. Chandler, and L. Zhang, *Optical Effects of Ion Implantation* (Cambridge University Press, Cambridge, U.K., 1994) p. 49.
- 54) C. Duan, P. A. Tanner, V. N. Makhov, and M. Kirm, *Phys. Rev. B* **75**, 195130 (2007).